THE ASTRONOMICAL JOURNAL VOLUME 105, NUMBER 5 MAY 1993

LINE PROFILE VARIATIONS IN M GIANTS: CLUES TO MASS-LOSS AND CHROMOSPHERIC HEATING MECHANISMS[1]

P. G. JUDGE

High Altitude Observatory, National Center for Atmospheric Research,[2] P.O. Box 3000, Boulder, Colorado 80307
Electronic mail: judge@hao.ucar.edu

D. G. LUTTERMOSER[3]

Department of Physics & Astronomy, Iowa State University, Ames, Iowa 50011
Electronic mail: lutter@fester.physics.iastate.edu

D. H. NEFF

National Optical Astronomy Observatories, P.O. Box 26732, Tucson, Arizona 85726-6732
Electronic mail: neff@vela.tuc.noao.edu

M. CUNTZ

High Altitude Observatory, National Center for Atmospheric Research, P.O. Box 3000, Boulder, Colorado 80307
Electronic mail: cuntz@hao.colorado.edu

R. E. STENCEL

Department of Physics, University of Michigan, 500 E. University Ave., Ann Arbor, Michigan 48109
Electronic mail: stencel@mich.physics.lsa.umich.edu

Received 1992 February 27; revised 1993 January 11

ABSTRACT

We analyze time-series, high dispersion spectra of the Mg II h and k and Ca II H and K lines of the semiregular giants ρ Per (M4 II–III, periodicity $P\sim 50$ days), R Lyr (M5 III, $P\sim 46$ days), and g Her (M6 III, $P\sim 90$ days). The targets were strategically selected to study the relative importance of convective motions and global stellar pulsations in determining the structure of the outer atmospheres. These first or second ascent stars lie in a crucial region of the HR diagram where circumstellar dust shells begin to form. We relate line profile variations to photospheric variations using the Fine Error Sensor on the *IUE* satellite and ground-based *UBV* photometry. We have detected small amplitude (typically $\pm 10\%$) but real changes in the profiles of Mg II and Ca II lines in all three stars which are not obviously related to underlying changes in the photospheres. We argue that the observed variability is due to changes in chromospheric conditions and not variations within the circumstellar shell. The observations support the picture of a steady-state "chromosphere" which is modulated on long time scales ($\sim$weeks). In g Her, we find evidence for a localized heating event which we tentatively assign to the overshooting of a large supergranule cell. Unfortunately, some important conclusions of related work by Eaton *et al.* [ApJ, 364, 259 (1990)] warrant a re-examination in the light of our analysis. We conclude that the geometric scales over which most of the energy is deposited in the outer atmospheres must be much less than a stellar radius, in contrast to large amplitude variables which are only slightly more evolved.

1. INTRODUCTION

A long-standing problem of stellar astrophysics remains the identification of the physical processes responsible for the chromospheres, coronae, and winds of cool stars (see Ulmschneider *et al.* 1991; Holzer & MacGregor 1985). There are several sources of energy and momentum which are considered to be important, depending on a star's mass and evolutionary history (e.g., Jordan & Linsky 1987; Jura 1986): (i) Magnetic fields generated in subphotospheric convection zones. (ii) Acoustic waves generated by the convection zones. (iii) Shock waves generated by global stellar pulsations. (iv) Force of photospheric radiation on circumstellar dust.

One way to examine the relative importance of these mechanisms is to study the variability of spectral features formed in the photospheres, chromospheres, and winds, since each of the above mechanisms operates on specific time scales and the energy and momentum propagates at specific velocities.

[1]Based on observations obtained with the *International Ultraviolet Explorer Satellite* at the NASA-Goddard Space Flight Center tracking station.

[2]The National Center for Atmospheric Research is sponsored by the National Science Foundation.

[3]Visiting Astronomer, Kitt Peak National Observatory and National Solar Observatory, NOAO, operated by the Association of Universities for Research in Astronomy, Inc. (AURA), under cooperative agreement with the National Science Foundation.

 0004-6256/93/051973-14$00.90

The aim of the present paper is to study chromospheric heating and mass loss in three strategically selected giant stars: ρ Per, R Lyr, and g Her. These stars lie in a region of the Hertzsprung–Russell (HR) diagram where small amplitude ($\Delta V \leqslant 3$ mag) photospheric variability is observed, and where circumstellar dust shells become evident. These stars are candidates for nonmagnetic processes, since they have "basal" chromospheric line fluxes (Schrijver 1987; Johnson 1987; Judge & Stencel 1991). They are also potential candidates for stars whose winds are driven by the action of waves generated by global pulsations (Bowen 1988). These targets therefore permit us to study the relative roles played by convective motions, global stellar pulsations, and dust in determining the structure of the outer atmospheres, in a crucial region of the HR diagram.

Eaton *et al.* (1990) have presented a variability study of similar stars, based primarily upon low dispersion spectra and upon an analysis of the integrated fluxes of emission lines. Several studies of high and low dispersion *IUE* data of the supergiant α Ori (M2 Iab) have been made (e.g., Dupree *et al.* 1988; Jorås 1989), again based exclusively on integrated line fluxes and other integrated or average quantities of the emission lines. The present paper's primary emphasis is upon the variability of line *profiles* and their relationship to theoretical models of chromospheric heating and mass loss. To our knowledge, this is the first study to analyze the observed profiles in detail.

Before proceeding, we wish to clarify our terminology. Judge & Stencel (1991) have argued that the traditional picture of a geometrically thin "solarlike" chromosphere (e.g., Athay 1976) might not be useful when applied to these evolved giants. We consider the "chromospheres" of these stars to be dynamical regions above the photosphere with characteristic temperatures between the radiative equilibrium temperature and roughly 10^4 K. The relationship between these "chromospheres" and the stellar "winds" observed in cooler spectral diagnostics (e.g., dust emission, sub-mm CO emission), is not yet clear, and is an important aim of this study. Both theory and observations suggest that they are physically connected since the "chromosphere" might be the region where the wind is accelerated in cool giants and supergiants (Goldberg 1979; Holzer & MacGregor 1985; Judge & Stencel 1991).

In Sec. 2 we discuss our target stars. Section 3 addresses our observations and data reduction. In Sec. 4 we describe the changes seen in the observed profiles and relate them to changes in the photospheric fluxes of the stars. Section 5 discusses implications for chromospheric heating and mass-loss mechanisms.

2. TARGET STARS

Our targets, ρ Per, R Lyr, and g Her, were selected using the following criteria: (i) They are late-M giant stars with small amplitude ($\Delta V < 3.0$ mag), semiregular photometric variations. (ii) They are all bright enough to permit observations at high dispersion with *IUE* (Eaton & Johnson 1988; Eaton *et al.* 1990). (iii) They do not possess optically thick dust shells, as indicated by their far-infrared colors (Judge 1989). (iv) Previous *IUE* observations have revealed detectable and significant variability in the Mg II h and k lines.

TABLE 1. Fundamental data for our target stars and photometric comparisons.

Star	ρ Per	R Lyr	g Her
Property ...			
Spectrum	M4 II-III	M5 III	M6 III
d [pc]	82	100	250
$T_{\rm eff}$ [K]	3500	3394	3250
$L_{\rm bol}/L_\odot$	2.3(3)[a]	3.7(3)	1.9(4)
$\mathscr{M}/\mathscr{M}_\odot$	5	2	4
$R/R_\odot$	1.5(2)	2.1(2)	6.3(2)
Variability[b] ...			
Type	SRb	SRb	SRb
$V_{\rm min}$–$V_{\rm max}$ [mag]	3.3–4.0	3.9–5.0	4.3–6.3
Periodicity [days]	50:	46	89.2
Circumstellar shell...			
[12]–[25][c] [mag]	−1.47	−1.45	−1.17
[25]–[60][c] [mag]	−1.92	−1.85	−2.0
$-d\mathscr{M}/dt$ [$\mathscr{M}_\odot$ yr^{-1}]	1.2(−8)	1.4(−8)	1.3(−7)
v_∞ [km s^{-1}]	7.5	7.0	10
Comparison stars ...			
HD number	19656	175740	150997
Spectrum	K0 III	G8 III	G8 IIIb
U,B,V [mag]	6.77,5.74,4.63	7.03[d],6.43,5.44	5.05,4.45,3.53

Notes to TABLE 1

[a] $x.y(z) \equiv x.y \times 10^z$. Data are from Judge & Stencel (1991) except:
[b] Variability data are from the *General Catalog of Variable Stars* (Kholopov *et al.* 1985).
[c] *IRAS* colors. $[12]–[25] \equiv -2.5 \log_{10}(F_{12}/F_{25})$, where, e.g., F_{12} is the flux in the 12 μm band, not color corrected, from the *IRAS Point Source Catalogue*. *UBV* colors (on Johnson's system) are from *The Bright Star Catalog* (Hoffleit & Jaschek 1984), except d whose U magnitude was estimated from the colors of the comparison star HD150997 of g Her.

Table 1 lists characteristics of these stars, with the three stars used as photometric comparisons. The table includes *IRAS* colors [12]–[25] and [25]–[60], taken from the *IRAS Point Source Catalog*, where $[\lambda] = -2.5 \log_{10} F_\lambda$, F_λ is the monochromatic flux at wavelength λ (microns). Neither ρ Per nor R Lyr shows evidence of a substantial dust shell either in these colors or in the LRS spectra. g Her does possess a rather thin dust shell (Judge 1989), of comparable thickness to a shell surrounding a typical Mira with a low mass-loss rate ($\sim 10^{-7}\,\mathscr{M}_\odot$ yr^{-1}, e.g., van der Veen & Habing 1988).

Fundamental stellar data are not well known but they have been estimated by Judge & Stencel (1991). They suggest that ρ Per and R Lyr are either at the tip of their first ascent of the giant branch (FGB) or beginning their ascent of the asymptotic giant branch (AGB). The estimated luminosity of g Her is consistent only with an intermediate mass star on the AGB. None of the stars can be in late phases of the AGB since they lack optically thick dust shells (van der Veen & Habing 1988).

TABLE 2. Log of *IUE* observations.

Star/Image	Disp.	Exp. time	FES counts[a] (Target)	FES counts (Comparison)	Date[b] JD' day
ρ Per					
LWP 16069	HI	13m	1113	265	7743
LWP 16104	HI	15m	1159	...	7750
LWP 16171	HI	15m	1190	...	7757
LWP 16213	HI	12m	1182	...	7764
LWP 16214	LO	45s			7764
LWP 16270	HI	12m	1145	269	7771
LWP 16310	LO	50s	1212	266	7778
LWP 16311	HI	10m			7778
LWP 16364	HI	11m	1234	257	7784
LWP 16410	HI	12m	1174		7792
LWP 16456	HI	12m	1158	24406[c]	7799
R Lyr					
LWP 15847	HI	20m	763		7711
LWP 15940	HI	20m	710	13032[c]	7723
LWP 16016	LO	2m	698	12679[c]	7736
LWP 16017	HI	20m			7736
LWP 16070	HI	20m	736	11906[c]	7743
LWP 16071	LO	2m			7743
LWP 16103	HI	20m	789	...	7750
LWP 16212	HI	20m	813	12530[c]	7764
LWP 16409	HI	20m	628	12736[c]	7792
LWP 16457	LO	2m	696	...	7799
g Her					
LWP 15845	HI	40m	441	724	7711
LWP 15846	LO	4m			7711
LWP 15939	HI	55m	436	745	7723
LWP 16015	HI	55m	437	741	7736
LWP 16102	HI	55m	442	749	7750
LWP 16170	HI	70m	443	753	7757
LWP 16269	HI	55m	467	732	7771
LWP 16312	HI	70m	455	...	7778
LWP 16365	LO	5m	449	731	7784
LWP 16366	LO	10m			7784
LWP 16367	LO	5m			7784
LWP 16411	LO	5m	449	...	7792
LWP 16458	LO	5m	457	...	7799

Notes to TABLE 2

[a]FES counts in the fast track underlap mode.
[b]Date=Julian Date −2 440 000=JD' as used in the text.
[c]FES counts in the fast track overlap mode.

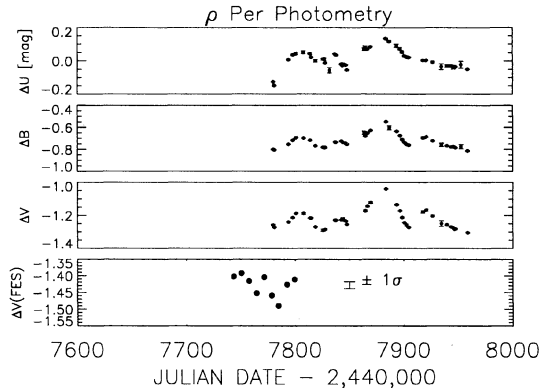

FIG. 1. Ground-based photometry and *IUE* FES photometry for ρ Per. The *V* magnitudes are given as *V*(target) − *V*(comparison) from both the Phoenix-10 telescope and from the FES photometry computed as described by Fireman & Imhoff (1989). Increasing ordinate values therefore imply decreasing brightnesses. Both datasets are normalized to the same comparison star. Error bars for *UBV* colors are internal errors—total standard errors are near 0.01 mag (see text). The offsets (~0.2 mag) between the *UBV* and FES data result from the color-dependent sensitivity of the FES.

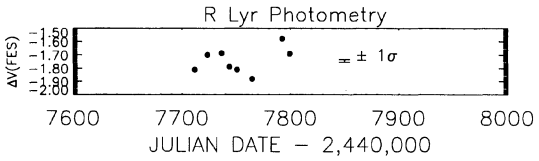

FIG. 2. Photometric data for R Lyr plotted as in Fig. 1. No *UBV* data were obtained for this star during the *IUE* observing period.

3. OBSERVATIONS AND DATA REDUCTION

3.1 Photometry

UBV photometry (on Johnson's system) was obtained from the Phoenix 10 automatic photoelectric telescope (APT) on Mt. Hopkins. Unfortunately this telescope was switched off during the summer of 1989 to avoid lightning damage, when the majority of our *IUE* observations were made. However, some data were obtained before and after our *IUE* run.

Table 2 lists the *IUE* observing log, including Fine Error Sensor (FES) counts for the targets and comparison stars. The FES provides an estimate of the Johnson *V* magnitude for stars which are not too red (Imhoff 1989; Fireman & Imhoff 1989). The wavelength sensitivity of the FES is known (Imhoff 1989), and for our targets the FES yields magnitudes which are closer to Johnson's *R* magnitude than *V*, even after applying the standard color correction (Fireman & Imhoff 1989). This accounts for systematic differences between FES magnitudes and the Johnson *V* magnitudes. Where no FES counts of a comparison star of a particular target were made on a given date, the other comparison stars were used as standards.

The derived *UBV* and FES magnitudes relative to the comparison stars are plotted in Figs. 1–3. The internal standard errors in the *UBV* colors which are plotted (⩽0.01 mag) are negligible in comparison with the observed variations. The standard errors of *V*(comparison)–*V*(check) are ~0.01 mag. The 1σ uncertainties in the differential FES magnitudes are ~0.01 mag (see Guinan 1990, Fig. 16). These uncertainties are much smaller than uncertainties of ~0.08 mag which arise if no comparison star is used (e.g., Fireman & Imhoff 1989).

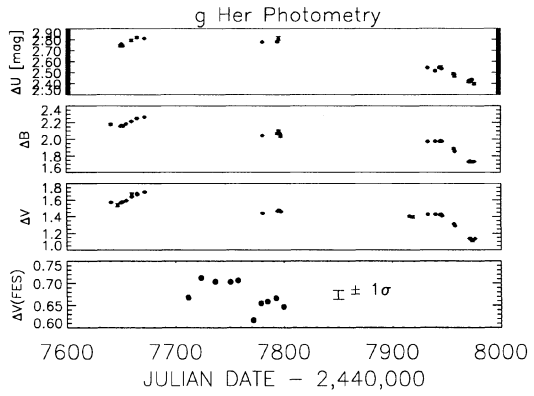

FIG. 3. Photometric data for g Her plotted as in Fig. 1.

For ρ Per the FES data provide evidence for photospheric variability ($\pm 6\sigma$ peak-to-peak amplitude). The agreement between the FES and APT data at the end of the *IUE* observing run confirms that the FES has indeed detected a maximum in visual light near JD-2 440 000 $\equiv$ JD' $\simeq$ 7780. The periodicity of the APT data suggests a typical time scale near 43 days, in reasonable agreement with the 40 day periodicity quoted in Table 1. For R Lyr the FES shows convincing evidence for systematic changes in visual light, with a maximum occurring somewhere near JD' = 7765. For g Her, the FES data show an approximate maximum light near JD' = 7770 days. The APT data were not obtained at suitable epochs for comparison with the FES data.

All three stars show smaller peak-to-peak photometric variations than those given in Table 1. We would expect to find a greater variation if we observed the stars for longer periods, as shown by the *UBV* measurements.

3.2 *IUE* Spectra

Spectra were obtained using the long-wavelength prime (LWP) camera through the large aperture ($\sim 10 \times 20$ arcsec), at both high and low dispersion, during 12 half-US2 shifts (Table 2). In some cases, only low dispersion data were obtained because of unusually high background radiation.

Exposure times were chosen to optimize the signal-to-noise ratio of the peak of the k line (the brightest feature in these spectra). The low-dispersion data have weak continua and show clearly just the h and k lines in emission. The high dispersion data show little continuum emission and other narrow emission lines of Al II] and Fe I near or below a 3σ level, as well as Mg II h and k.

The spectra were reduced using IDL software at the *IUE*-RDAF at the University of Colorado. The basic data consist of the extracted spectra from the standard IUESIPS (version 2) reductions. These include wavelength corrections for the Earth's radial velocity. The low dispersion data were measured to derive the total flux (erg cm^{-2} s^{-1}) in the Mg II h and k lines, $F(\mathrm{h+k})$, integrated over the whole feature at 2800 Å. The high dispersion spectra were also measured to obtain $F(\mathrm{h+k})$, but in addition the spectra were processed in order to highlight the Mg II h and k line profile variations. We adopted the following procedure.

First, the photowrites (photographic reproductions of the raw *IUE* echelle image) were examined to identify image flaws (particle hits, reseau marks). There is a reseau mark lying close to the red wing of the k line. This influences just a few pixels in one interorder "background" channel and so its effects were neglected here. Next we measured the wavelengths of weak features in the high dispersion spectra to correct for pointing errors and systematic wavelength shifts in the large aperture. We used lines of small optical depth (Al II] λ2669.166) and other lines whose emission cores are formed in the deep layers of the chromosphere (Fe I $\lambda\lambda$ 2823.276, 2843.977, Harper 1990) which are definitely present on the photowrites to determine the magnitude of possible wavelength shifts. The shifts were determined from the Al II] and Fe I lines with sufficient signal-to-noise ratios. The shifts (converted to Doppler units of km s^{-1}) are given as V_L in Table 3. We then measured the total fluxes in the h and k lines using direct integration over the line profiles, and in the lines of Al II] and Fe I where the peak signal-to-noise ratio was sufficient ($\geqslant 2$). Gaussian profiles were fitted to these lines to derive the integrated line fluxes and centroid velocities listed in Table 3.

TABLE 3. Measurements of emission lines.

Star/Image	F(k)	F(h)	F(λ2669)	F(λ2823)	F(λ2843)	V_L^c
	10^{-13} erg cm^{-2} s^{-1}					km s^{-1}
ρ Per						
16069	255	175	11	11	10	33
16104	257	167	16	10	9	28
16213	253	169	15	14	11	36
16214	373[a]	...	...	...	...	...
16270	252	178	13	11	12	36
16310	>273[a]	...	...	...	...	...
16311	231	168	14	8	10	34
16364	226	129	9	9	7	37
16410	200	125	8	10	9	37
16456	225	128	14	11	14	...
mean $\pm 1\sigma$[b]	240±21	159±24	12.4±2.7	10.3±1.8	10.7±2.4	32.9±5.3
R Lyr						
15847	128	78	...	7.5	3.1	-14
15940	120	71	...	5.8	4.1	-14
16016	172[a]	...	...	...	...	...
16017	118	73	...	6.3	3.3	-23
16070	122	83	...	4.4	3.7	-28
16071	>181[a]	...	...	...	...	...
16103	119	79	...	6.7	3.5	-27
16212	112	78	...	7.0	4.1	-18
16409	124	74	4.4	4.2	3.3	-21
16457	173[a]	...	...	...	...	...
mean $\pm 1\sigma$[b]	120±5	77±4	...	5.9±1.3	3.5±0.4	-20.7±5.7
g Her						
15845	30.0	15.0	...	1.5	1.2	19
15846	39.3[a]	...	...	...	...	...
15939	27.0	14.0	...	1.2	1.0	24
16015	27.0	17.0	...	1.4	0.5	28
16102	26.0	16.0	1.7	1.5	0.8	24
16170	27.0	17.0	...	1.4	...	...
16269	34.0	17.0	1.1	1.6	1.5	11
16312	30.0	17.0	1.2	1.5	1.5	24
16365	41.1[a]	...	...	...	...	...
16366	>40.1[a]	...	...	...	...	...
16367	42.0[a]	...	...	...	...	...
16411	40.6[a]	...	...	...	...	...
16458	>41.6[a]	...	...	...	...	...
mean $\pm 1\sigma$[b]	28.7±2.8	16.1±1.2	...	1.4±0.1	1.1±0.5	21.7±6.0

Notes to TABLE 3

[a]Low dispersion data. Mg II h+k fluxes are tabulated.
[b]Means of high dispersion data only.
[c]Measured velocity shift of the weak lines of Al II and Fe I.

We then constructed "mean" spectra of the h and k lines by taking the unweighted mean of the high dispersion spectra for each star, with wavelengths scales aligned to correct for the measured velocity shifts (the tabulated values of V_L were subtracted from the observed velocity shifts for each spectrum). The mean spectra were subtracted from the individual spectra to highlight the differences between the line profiles as a function of time. The results of these reduction procedures are given in Table 3 and in Figs. 4–8. These form the basis of the remaining discussion.

The photospheric radial velocities of ρ Per, R Lyr, and

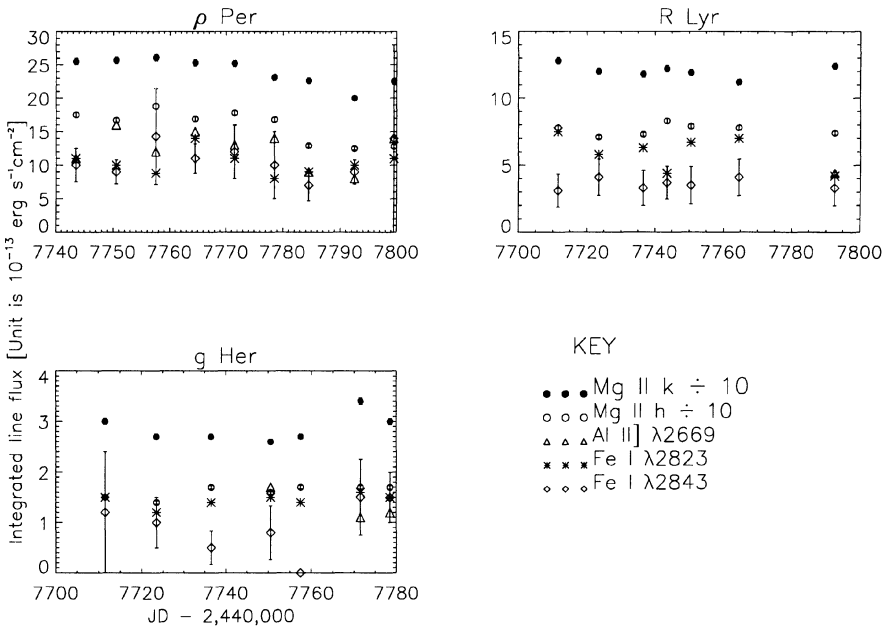

FIG. 4. Variations in the integrated fluxes of the Mg II, Fe I, and Al II] lines in the time series spectra of ρ Per, R Lyr, and g Her. Relative uncertainties in the fluxes of the well-exposed Mg II lines are small (a few percent at most). Lower limits to the standard errors for h and k are shown, based upon the photometric reproduceability of the echelle mode of *IUE* (see text). Standard errors for the weaker lines are represented by those plotted for Fe I λ2843. The flux scale is in units of 10^{-13} erg cm^{-2} s^{-1}.

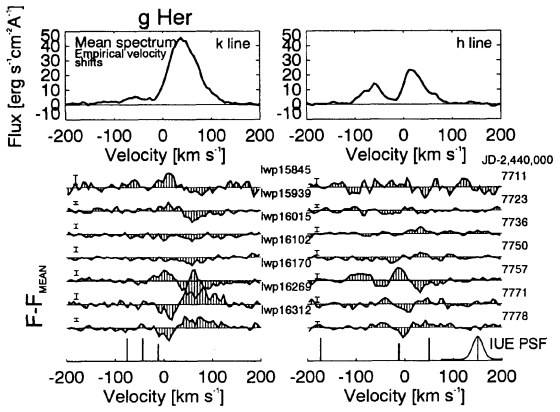

FIG. 5. Spectra of the Mg II h and k lines obtained in the time-series observations of g Her. The top panel shows the "mean" spectrum obtained by an unweighted average of the individual spectra. The ordinate is monochromatic flux in units of 10^{-13} erg cm^{-2} s^{-1} Å^{-1}. The abscissa is the Doppler shift in km s^{-1}, on a scale where V_L is set to zero (see the text and Table 3). Note that for optically thick lines such as Mg II h and k these velocities do not represent directly the actual gas motions, since the line broadening is determined by scattering of photons at high line center optical depths. The lower panels show the difference between the individual spectra and the mean spectrum, with flux differences magnified by a factor of 2 for clarity. The $\pm 1\sigma$ error bars were computed from the standard deviations of the fluxes between the (absolute) Doppler shift velocities of 150 and 250 km s^{-1}. The long and short vertical lines show the expected positions of the circumstellar and interstellar absorbers respectively (see text). The *IUE* point spread function (*IUE* PSF) is also shown.

g Her are +28.2, −28.3, and +3.4 km s^{-1}, respectively (from the *General Catalog of Radial Velocities*). The mean radial velocities determined from the Fe I lines are, for ρ Per and R Lyr, in rough agreement with the stellar radial velocities, given measured standard errors of 5–6 km s^{-1}. Such errors are typical of the variations expected from the limited accuracy with which the *IUE* spacecraft can place a target in the large aperture (± 1 arcsec; Ayres 1991). These uncertainties represent the limiting precision with which we could align the spectra from different exposures on top of one another.

For g Her, the mean radial velocity determined from the Fe I lines is redshifted by 18.3 km s^{-1}, a 3σ deviation,

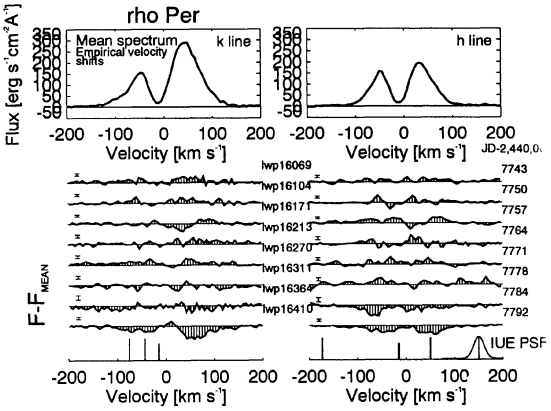

FIG. 6. Line profile data for ρ Per plotted as in Fig. 5.

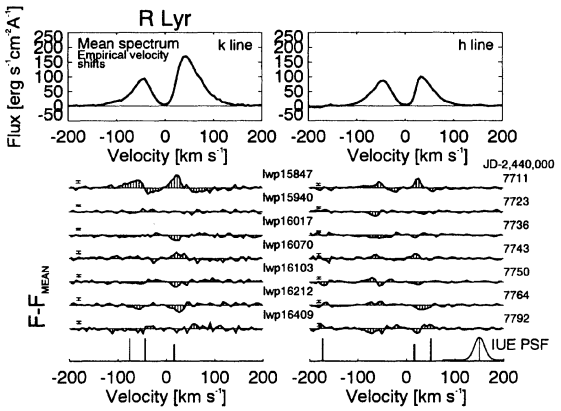

FIG. 7. Line profile data for R Lyr plotted as in Fig. 5.

from the photospheric radial velocity. The Al II] λ2669.166 line (which was definitely detected only in image LWP16102), is redshifted only by roughly 9 km s^{-1}, relative to the photospheric velocity. This indicates that a radiative transfer effect (scattering of Fe I photons in the blueshifted absorption lines in the stellar wind, for example) may be responsible for the redshift in the Fe I lines.

3.3 Ground-Based Spectra

Near-simultaneous observations were obtained in the Ca II H and K spectral region, primarily with the National Solar Observatory's (NSO) McMath telescope on Kitt Peak. One spectrum obtained at the McDonald Observatory was kindly supplied to us by Dr. V. Smith of the University of Texas (Table 4).

The McMath data were obtained both under the NSO guest observing (program #1451) and the synoptic (#1468) programs. The McMath telescope focuses an $f/54$ beam with an image scale of 2.54 arcsec/mm onto a

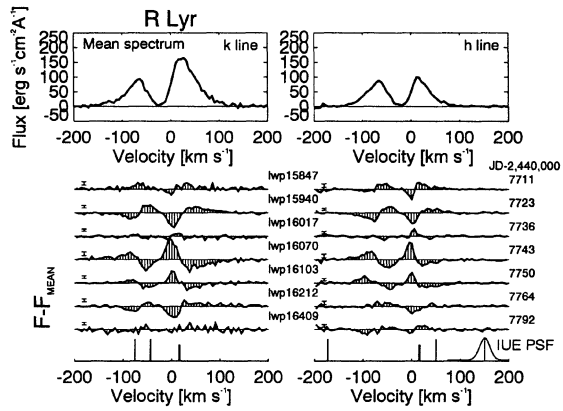

FIG. 8. Identical figure to Fig. 7 except that the empirical velocity corrections to the wavelength scales were replaced by the stellar radial velocity. Comparing this plot with Fig. 7 reveals the importance of matching the wavelengths scales accurately if reliable line profile variability information is to be derived.

TABLE 4. Ca II H and K observations.[a]

Star	JD′ [b] day	Exposure time (min)	Spectral resolution (km/s)	S/N [c]
ρ Per	7752	60	10	60
	7765	40	14	65
	7771	45	14	90
	7784	20	15	190
R Lyr	7750	60	10	40
	7764	60	14	75
g Her	7750	60	10	30
	7751	150	10	50
	7763	60	14	50

Notes to TABLE 4

[a]Observations taken with the NSO McMath telescope except ρ Per (JD′=7784) which was taken with the McDonald telescope.
[b]Add 2,440,000 to tabulated number to obtain Julian Date.
[c]Signal-to-noise (S/N) evaluated in the Ca II H&K line cores.

5-slice internally-reflecting Bowen–Walraven image slicer (Jaksha 1989). A Milton and Roy III (i.e., blue) grating was used in conjunction with a Schott BG-3 filter to block unwanted spectral orders. The detector was a TI-4 800 $\times$800 thinned UV enhanced CCD. Guiding was performed directly from the target star via a thin broadband dichroic mirror over the image slicer. A Kinoptic transfer lens with a resolution $\lambda/\Delta\lambda$ of 22 000 was used for half of the McMath observations, and a 180 mm lens ($\lambda/\Delta\lambda$ =30 000) for the other half producing slightly different spectral resolutions. Table 4 summarizes our Ca II observations.

Figures 9–11 show the Ca II H and K line cores for g Her, ρ Per, and R Lyr, respectively. Flat-fielding and bias subtraction were made with the SPECPROC spectral reduction package at NSO. Wavelength calibrations were performed using IDL software at the University of Colorado, based on a χ^2 minimization technique of a linear least-squares fit to the comparison lamp spectrum. The Earth's and stellar radial velocities have been subtracted out in the wavelength calibration. One-sigma errors in the wavelength calibration range between 1 and 2 km s^{-1} (expressed as a Doppler shift). The spectra are normalized by the exposure time of the observation and scaled to an "arbitrary" flux proportional to the CCD ADU. Successive spectra for a given star are shown stacked, separated by "one" (three in the case of ρ Per) arbitrary flux unit. We plot these spectra as a function of velocity shift with respect to line center (i.e., $v=c\Delta\lambda/\lambda$). Note that radiation hits are marked with an asterisk. The bars on the right-hand side of each spectrum represents the spectral resolution (horizontal line, note that the 1σ wavelength error is much less than the resolution) and estimated noise (vertical line), which is based on the theoretical signal-to-noise ratio of the TI-4 chip (Jaksha 1989). The full length of the vertical "noise" line corresponds to the 2σ level for the region of the Ca II H and K line core fluxes.

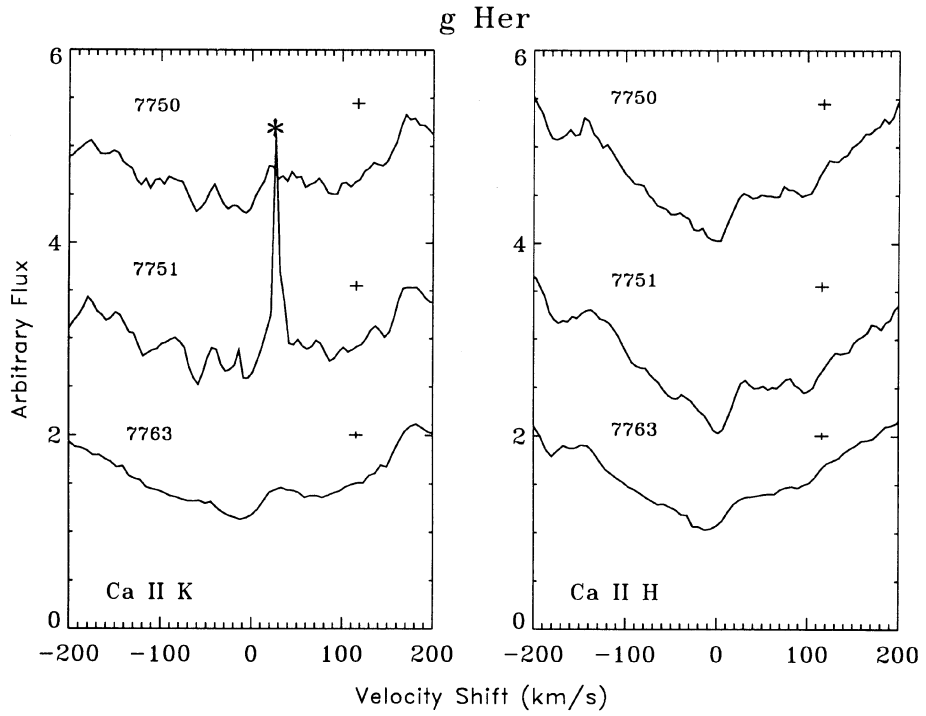

FIG. 9. A series of Ca II K and H line-core spectra of g Her labeled by JD′=Julian Date−2 440 000. The "crosshairs" on the right-hand side of each spectrum corresponds to size of the spectral resolution (horizontal line) and the instrumental noise (vertical line, full length=2σ). Cosmic ray hits are indicated with an asterisk. Spectra are offset from one another by 1 arbitrary flux unit.

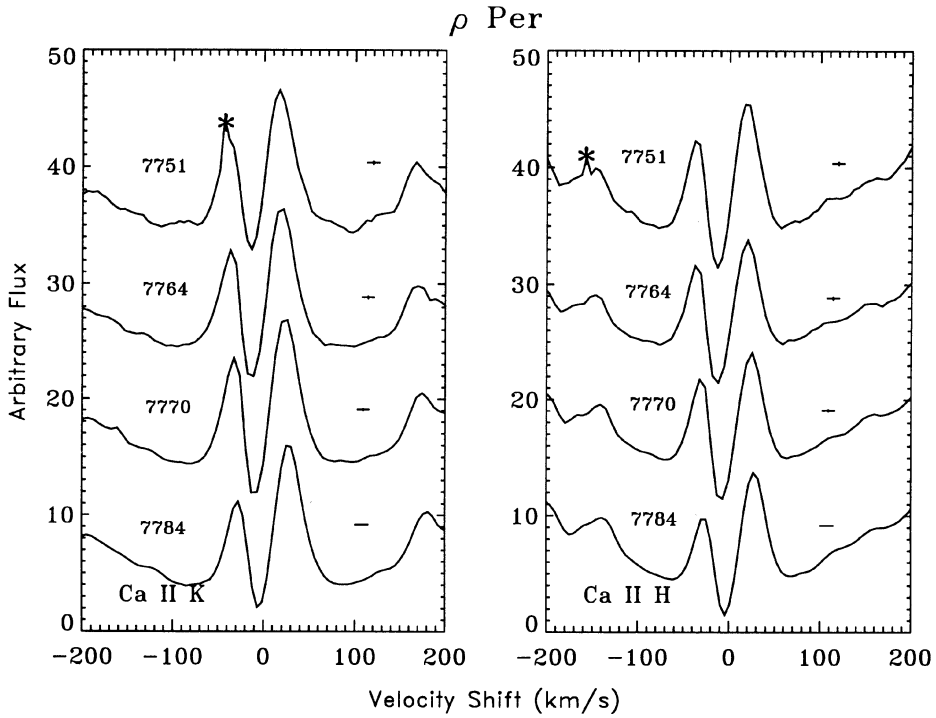

FIG. 10. Ca II H and K spectra of ρ Per. Figure labels are the same as Fig. 9, except the spectra are offset from one another by 3 arbitrary flux units.

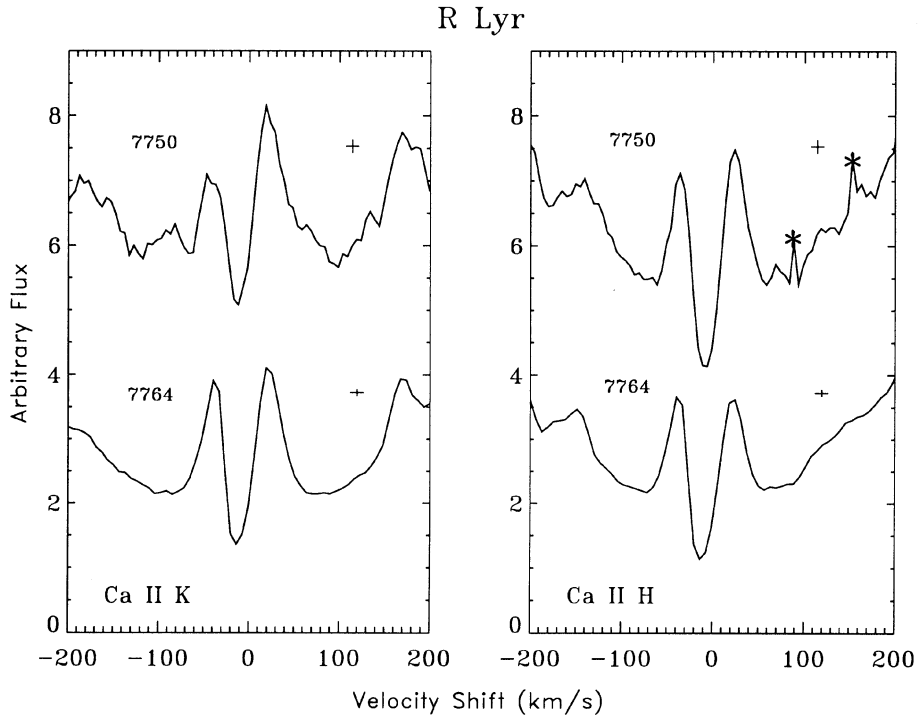

FIG. 11. Ca II H and K spectra of R Lyr. Figure labels are the same as Fig. 9.

4. LINE VARIABILITY

4.1 Integrated Line Fluxes

Figure 4 shows the time variation of the integrated fluxes $F_\oplus = \int_{\Delta\lambda}(F_\lambda - F_c)d\lambda$ of the emission lines minus (weak) continuum flux F_c. The figure does not show low-dispersion data, which are systematically a factor of ~ 0.88 smaller than the high dispersion data for reasons which are not clear (Taylor 1990).

The error bars for $F_\oplus$ (Fe I λ2843) have been estimated from the signal-to-noise ratio of the line in each spectrum. These estimates contain only relative uncertainties and do not include absolute uncertainties (e.g., in the flux calibration). Error bars for Fe I λ2823 and the Al II] λ2669 are larger than for Fe I λ2843. Relative standard errors in the Mg II *integrated* line fluxes (i.e., sums over many individual pixels) are $\sim 2\%$, based upon the reproduceability of continuum fluxes in echelle data of Capella by Ayres (1984). These error estimates are plotted in Fig. 4. We note the following properties which are common to all three stars.

(i) There are significant changes in $F_\oplus$(h+k): $\sim \pm 4\%$ in R Lyr and $\sim \pm 10\%$ in both ρ Per and g Her. (ii) These changes are not obviously related to the changes in the V-band fluxes (see Figs. 1–4), which have amplitudes

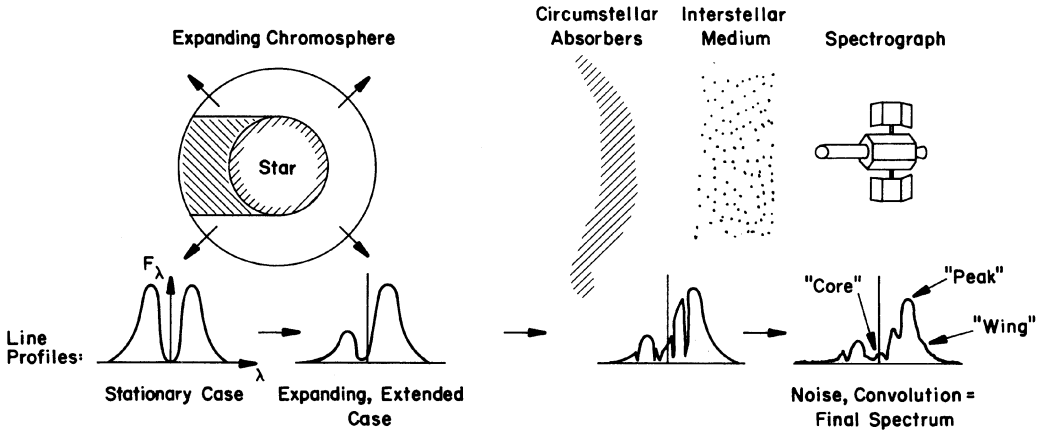

FIG. 12. Figure illustrating physical and instrumental effects influencing the observed profiles.

TABLE 5. Known circumstellar and interstellar absorption features in the region of the Mg II resonance lines.

Line	λ (Å)	ΔV [a] (km s^{-1})	Mg II line	E_l [b] (eV)	τ_{10} [c]	Source
Mn I	2794.817	−76	k	0.00	70	Bernat & Lambert (1976)
Fe I	2795.006	−55	k	0.00	4.0	Bernat & Lambert (1976)
Mn I	2801.08	−173	h	0.00	40	Eriksson *et al.* (1986)
Fe I	2803.169	+50	h	0.05	$\leqslant$1.3 [d]	Bernat & Lambert (1976)

Notes to TABLE 5

[a]ΔV is difference in rest wavelengths between the absorber and the listed Mg II line, expressed in Doppler shifts from the center of the Mg II line.
[b]Excitation energy of the lower level of the transition in eV.
[c]Order of magnitude estimates of the optical depth at the center of the circumstellar line between the observer and a surface at 10 stellar radii from the stellar center, for the case of g Her (see text). For ρ Per and R Lyr these estimates are both a factor of two smaller than those listed.
[d]Upper limit determined by setting the Boltzmann factor $\exp(-eE_l/kT_e)=1$.

$\sim\pm9\%$ in R Lyr and $\sim\pm3\%$ in both ρ Per and g Her. In R Lyr, the V-band flux varied significantly more than the Mg II line fluxes. (iii) There is no clear evidence of a time lag between the V magnitude and the chromospheric emission. However, if a time lag of several weeks were present, similar to that found for W Cyg and NU Pav by Eaton *et al.* (1990), we would not have detected it. (iv) The ratio $F_\oplus(\mathrm{h})/F_\oplus(\mathrm{k})$ changes significantly, most dramatically for g Her. (v) The Al II] and Fe I lines vary, within large uncertainties, together with the fluxes in the Mg II lines.

Point (v) contrasts with the findings of Eaton *et al.* (1990), based upon similar data for R Lyr. This is discussed further in Sec. *5.4*.

4.2 Line Profiles

4.2.1 Preliminary considerations

It is notationally convenient to define three regions of the line profiles (Fig. 12): the "wings," "peaks," and "cores" of the emission lines. In traditional notation (e.g., Athay 1976) the emission "wings" lie between components k_1 and k_2, the "peaks" correspond to k_2, and the "cores" to k_3 (and similarly for the h and Ca II lines). Using cosmic abundances (Allen 1973) and assuming that the dominant ionization stages are singly ionized, the Mg II and Ca II resonance lines have optical depths in the ratio k:h:K:H =26:13:2:1. Figure 12 illustrates a physical picture which we use to interpret the Mg II and Ca II profiles. We consider (as a starting point) a smooth, spherically symmetric, outflowing outer atmosphere. Several effects must be considered (Fig. 12).

(i) The emergent profile from a (ficticious) stationary atmosphere would be symmetric and self-reversed.

(ii) Both velocity fields and extended geometry introduce asymmetries into resonance line profiles (Drake & Linsky 1983; Drake 1985). For such optically thick lines in an expanding medium, the blue absorption components and peak emissions are formed mostly in front of the star, while the red emission peaks have components from both the front and far side of the star, as viewed from Earth.

(iii) The profiles are influenced by absorption in the circumstellar environment. Known absorbers (with lower excitation energies below a few hundred degrees Kelvin) are listed in Table 5. The positions of these absorbers are marked on Figs. 5–8. Potential absorbers over the Ca II lines have not yet been identified. The list of emission lines discussed by Stencel (1977) suggests that circumstellar and interstellar lines of abundant ions (e.g., Fe I) will be weak since the lower levels lie typically at energies $\geqslant$2 eV.

(iv) The interstellar medium (ISM) will scatter photons out of the line of sight. The velocities of Mg II and Ca II absorbers in the local ISM (within $\sim$50 pc) can be estimated using the "average" vector "G" of Drake *et al.* (1984). In the rest frames of the stellar photospheres, we expect to see local ISM absorption components near −15, +16, and −12 km s^{-1}, in ρ Per, R Lyr, and g Her, respectively. These velocities are also indicated on Figs. 5–8. Ca II is expected to have much weaker ISM absorption components than Mg II, with an equivalent width only $\sim$50 mÅ for stars at 300 pc (Hobbs 1974).

(v) The observed profiles are convolved with the point spread function of the *IUE* spectrograph. We can therefore reject any changes in the profiles whose widths (full width at half maximum flux) are less than 25 km s^{-1}.

4.2.2 Expected influence of circumstellar absorbers

No determinations of the equivalent widths of the circumstellar lines are available for these stars. However, we can estimate the influence of Fe I and Mn I circumstellar lines from the atomic parameters and from circumstellar column densities calculated from the (uncertain) gross wind properties (Table 1). As noted by Eriksson *et al.* (1986), the Mn I lines are expected to be formed near the "pure scattering" limit where all absorbed photons are re-emitted in the same multiplet. However, the Fe I lines are expected to be formed near the "pure absorption" limit where all absorbed photons are re-emitted in another multiplet. We therefore expect that detailed transfer calculations are required to estimate the influence of the Mn I lines,[4] but that the absorption due to Fe I lines can be well approximated by using a simple $\exp(-\tau_\nu)$ extinction law, where τ_ν is the optical depth in the line at frequency ν in the circumstellar shell.

[4]Some observational evidence for optically thick circumstellar absorption in Mn I lines in α Ori (M2 Iab) has been obtained with the Goddard High Resolution Spectrograph on the *Hubble Space Telescope*: Carpenter (1992) has presented fully resolved profiles of the Mg II h and k lines which show essentially black circumstellar absorption features in the circumstellar Mn I lines.

Table 5 lists line center optical depths τ_{10} in the circumstellar lines computed from the mass-loss rates and wind velocities of Table 1 at ten stellar radii from the star's center, together with oscillator strengths from Corliss & Tech (1968) for Fe I and from Younger *et al.* (1978) for Mn I. We made the following reasonable assumptions: (i) The wind speed is constant above ten stellar radii. (ii) Neither circumstellar iron nor manganese are significantly ionized. (iii) The Doppler broadening is ~ 5 km s^{-1}. (iv) Abundances are close to solar (we used those of Allen 1973).

These order-of-magnitude estimates of τ_{10} are of order unity or greater, showing that the lines can remove significant amounts of flux from the observed profiles. The lines are strong enough that they are not expected to be formed on the linear part of the curve of growth. This has two important consequences: (i) large changes in the circumstellar optical depths will not necessarily result in large changes in the observed emission line flux, and, (ii) large changes in the chromospheric emission near the centers of these circumstellar lines (slab calculations suggest within $\sim \pm 0.1$ Å $\equiv \pm 10$ km s^{-1}) will not be observable from earth.

4.2.3 Data for g Her

We discuss data for g Her first because the profile variations are simpler in this star. Inspection of Figs. 5 and 9 reveals the following.

(i) Real, statistically significant profile changes were observed at some epochs in spectra of the k line. These are seen in the core, red peak, and red wing.

(ii) Corresponding changes in the h line are not always detected, owing partially to the lower signal in the h line.

(iii) g Her shows only subtle changes in the cores of H and K.

(iv) No significant changes occurred in the blue wing of the k line ($V \leqslant -40$ km s^{-1}), even when significant changes occurred in the h line at corresponding velocities (see LWP16170). This suggests that the k line absorbers (Table 5) are so strong that little flux emerges at these wavelengths. Furthermore, the observed changes in the h line must occur in layers deeper than the circumstellar shell.

(v) Between JD′=7757 and 7771, an $\sim 25\%$ (10σ) increase occurred in the red peak/wing of k line but not the h line. The reality of this change cannot be doubted since the increased flux survives the empirical velocity-shifting procedure (which cannot influence the integrated line flux), and the photowrite is very clean. The FES flux increased only by 10%.

(vi) Evidence for *systematic* changes in the line profiles is seen in the core ($-20 < V < 20$ km s^{-1}) and red peak ($0 < V < +100$ km s^{-1}) of the k line. The line core was initially stronger than average ($\sim 3\sigma$), then weakened until JD′=7757 when the core became enhanced once again. This enhancement was more evident in the h line where a deviation of 6σ is observed, together with a 3σ enhancement in the blue wing of h. These differences between the h and k lines can *only* be accounted for by the masking effect of circumstellar lines overlying the k line.

(vii) The Ca II data (ignoring the radiation hit on JD′=7751) show that between JD′=7750 and JD′=7763, the line absorption core shifted from near 0 km s^{-1} to -10 km s^{-1}. This is similar to the behavior of the h and k lines at JD′=7750 and 7757, suggesting that the cause of the variations must be related to atmospheric changes which influence transfer of radiation in the Ca II and Mg II lines themselves, and not to the effects of other (unidentified) lines in the circumstellar shell.

Point (v) is a very significant result: in the absence of overlying absorbers in either line, the h line has to behave in a very similar manner to the k line. This is because both lines are excited by electron collisions, both are effectively thin in the chromosphere (Judge 1990), and they differ in optical depth only by a factor of two. We conclude that *the h line profile near the red peak and wing must be strongly influenced by overlying absorbers which mask underlying chromospheric variability*. In fact, in the mean h profile, there is a suggestion of a line absorber near $+60$ km s^{-1}, which lies close to the predicted velocity of $+50$ km s^{-1} for Fe I λ2803.169 (Table 5). The presence of such a strong absorber over the h line provides a natural explanation for the large change in the ratio of $F(\mathrm{k})/F(\mathrm{h})$ seen in Figs. 4 and 5. The inferred absorber may be stronger than estimated for the Fe I line given in Table 5, but given the large uncertainties in circumstellar optical depths, it is not in gross disagreement.

Furthermore, the absence of enhanced emission in the blue wing of the h line, expected (in spherical symmetry) on the basis of this enhanced emission observed in the red wing of the k line in spectrum LWP16269, suggests that the enhanced emission must also be localized geometrically somewhat behind the star. This is because the red wing is preferentially formed behind the star in spherically expanding models (Drake & Linsky 1983).

4.2.4 Data for ρ Per

Data for ρ Per are of substantially higher quality than for g Her, with the exception of LWP16456 which was obtained during a shift with exceptionally high levels of background radiation. The observed changes are marginal for this particular image and therefore we will ignore these data in our discussion.

A feature of the profile changes in ρ Per is that *statistically significant changes in the h line are accompanied by equivalent changes in the k line*. The changes occur farther from line center in k compared with h. This correlation suggests that the overlying absorbers in the circumstellar environment (cf. Table 5) are weaker than in g Her, as expected from the lower measured mass-loss rate of ρ Per (Table 1).

We find no evidence for changes in the line cores ($V \sim -10$ km s^{-1}), which suggests that the ISM might be a prominent contributor at these velocities (the local ISM is expected to be near -15 km s^{-1}). In contrast, the core velocities of Ca II H_3, K_3 tend to increase systematically with time from ~ -10 km s^{-1} at JD′=7751 to ~ 0 km s^{-1} (K_3) and ~ 5 km s^{-1} (H_3) at JD′=7784. This

TABLE 6. Time and length scale estimates for waves generated by global pulsations and "classical" convection.

Star	P_{CO} days	P_{MAX} days	$\epsilon=\lambda/R_*$	P_0	P_1	P_2	ΔT_{OBS}[a] days	$\int dT_{OBS}$[b] days
ρ Per	9	$\geqslant$2	0.01	46	25	19	7	56
R Lyr	33	$\geqslant$7	0.03	72	36	28	11	88
g Her	200	$\geqslant$40	0.06	260	105	80	9	88

Notes to TABLE 6

Uncertainties in the time scales are ± a factor of two (see text).
[a]Average interval between observations.
[b]Total observation period.

indicates that the Mg II h_3 and k_3 components are dominated by absorption in the ISM, but that the Ca II H_3 and K_3 components are formed in the stellar environment.

There is some indication that the Mg II red wings and peaks change substantially more than the blue wings and peaks. In most spectra, changes clearly present in the red peaks and wings are reflected in weaker changes in the blue peaks. These effects are more pronounced in the k line. These profile changes are not reflected by similar behavior of the Ca II lines, in which both the red and blue peaks show substantial variations. We conclude that circumstellar absorbers are sufficiently strong to influence the k profile between Doppler shifts of -80 and -50 km s^{-1} (Table 5) to mask chromospheric variations at these velocities.

Unlike g Her, the Fe I UV3 absorber overlying the h line seems to be less important since changes in the red and blue peaks of the h line are generally of similar magnitudes. This can be understood if the excitation temperature of the Fe I absorbers in the envelope of ρ Per is much below that of g Her. Bernat (1981) finds a value near 90 K for ρ Per, based upon CO lines, compared with an excitation energy which has a temperature equivalent to 600 K. We conclude that excitation temperatures of Fe I in the circumstellar shell of g Her must be on the order of a few hundred K.

4.2.5 Data for R Lyr

R Lyr showed disconcertingly large changes in the line profiles when corrections were made for the inaccurate placement of the star in the large aperture, because of steep gradients ($dF/d\lambda$) in the h and k profiles (compare Figs. 7 and 8). Under these conditions it is more difficult to believe the profile changes shown in Figs. 7 and 8 than in Figs. 5 and 6. However, the corrections have provided much smaller scatters in $F-F_{MEAN}$ and a much smoother (and hence more believable) mean profile. Therefore, we base our discussion upon the data shown in Fig. 7 only.

The two Ca II data show a very interesting behavior: the red and blue peaks of the H and K lines change substantially. The h and k spectra change in the same manner on the same dates. As we inferred for ρ Per, this behavior indicates that the profile changes must originate in deep layers of the chromosphere, and not in the circumstellar shell.

5. DISCUSSION

5.1 Overview of our Results

Our major results can be summarized as follows.

(i) Using the FES on board *IUE* is possible to detect 1σ changes in the "visual" magnitude (actually closer to Johnson's R than V) as small as 0.01 by using suitable comparison stars. The FES detected significant photospheric variability of ρ Per, R Lyr, and g Her.

(ii) *IUE* can easily detect variations in the integrated line fluxes of these targets. At high dispersion, we find changes in the k/h ratio.

(iii) The photospheric flux and Mg II integrated line flux variations are not obviously related in our time series, which approximately cover one cycle of the "periodicity" of these semiregular variables. In R Lyr the amplitude of visual flux variations is twice that of the Mg II lines.

(iv) Other UV emission line fluxes (Al II], Fe I) do not vary differently from the Mg II lines, to within large uncertainties. Below we discuss our results in relation to those of Eaton *et al.* (1990) who claimed (with reservations) that the "Al II [line flux] is not proportional to [the] Mg II [line flux]."

(v) To interpret profile variations in *IUE* spectra, care must be taken to align accurately spectra taken through the large aperture. Spurious variations result when wavelength scales are not aligned. We used weak lines of low optical depth, formed in deep layers of the chromosphere (Judge 1986; Harper 1990), as wavelength fiducials.

(vi) The largest changes in profiles generally occur near the "peaks" of the emission lines. Furthermore, there is a correlation between Ca II and Mg II profile changes in regions of the Mg II profiles where circumstellar absorbers are not expected to be strong. These points reveal that *the major source of the variability occurs in layers of the chromosphere much deeper than the circumstellar shell.*

(vii) Variations in the circumstellar line absorption properties were not detected in our dataset. This does not mean that the circumstellar properties (density, temperature) did not change significantly, since the absorption lines are expected to have optical depths greater than unity (Table 5), and changes in the circumstellar line optical depth $\Delta\tau$ will result only in small changes in equivalent widths ($\propto \sqrt{\ln \tau}$).

(viii) g Her, the star showing the largest changes, showed a 10σ increase in the red wing of the k line only.

This can be understood by a localized heating event occurring behind the star, above the limb.

(ix) From the behavior of the k and h lines at the wavelengths of the Fe I absorbers, we can infer that the circumstellar shell of ρ Per must have a substantially lower excitation temperature than that of g Her. The excitation temperature of ρ Per was previously measured to be 90 K (Bernat 1981).

5.2 Some Theoretical Time Scales

Here we investigate the assumption that purely nonmagnetic processes are responsible for the observed profile changes. (Of course, we cannot rule out solarlike magnetic variability, but our assumption seems worthwhile given the evidence summarized in Sec. 1). Table 6 lists some time scales for wave modes generated by convective motions and by pulsation modes, for comparison with our observations. P_0, P_1, and P_2 are fundamental, first, and second overtone periods which have been computed from the formulas of Lovy *et al.* (1984) based upon the data listed in Table 1.

P_{CO}, P_{MAX}, and ϵ are quantities related to the propagation of acoustic waves generated by the convective zone, based upon "classical" convective zone models (Bohn 1981; 1984). These models adopt time-independent mixing-length theory which is a poor description of the convective zone dynamics (e.g., Malagoli *et al.* 1990). Furthermore, earlier studies suggested that the sizes of convective cells might approach a stellar radius (Schwarzschild 1975; Antia *et al.* 1984) in low gravity stars. P_{CO} is the "acoustic cutoff period" estimated for regions near the top of the convection zone. Small amplitude outwardly propagating sound waves must have periods $P < P_{CO}$. $P_{MAX} \sim 1/5 P_{CO}$ is a theoretical estimate for the periods near which (a) the maximum of the wave energy spectrum is expected (Bohn 1981; 1984), and (b) stochastic heating events are expected, based upon theoretical calculations of Cuntz (1987). In the lower-middle chromosphere, P_{MAX} should be interpreted as a lower limit for time scales of the majority of stochastic heating events. Since all of these time scales vary proportional to gravity g^{α} where $\alpha \simeq -1$, these are uncertain by a factor of two (Judge & Stencel 1991). ϵ is the wavelength of a typical propagating shock wave expressed as a fraction of a stellar radius.

In Table 6 we also list the mean interval between observations ΔT_{OBS} and the total observing periods $\int dT_{OBS}$ for our three stars. Comparison of the theoretical time scales with ΔT_{OBS} reveals the following: for ρ Per and R Lyr, $1/P_{MAX} > \nu_{Ny} = 1/(2\Delta T_{OBS})$ where ν_{Ny} is the approximate Nyquist frequency for our datasets. Thus, we cannot determine high frequency profile changes arising from the predicted propagation of waves generated by the "classical" convection zone models in these stars. The observed variabilities in these stars must result from either (i) pulsation modes, (ii) larger-scale motions in the convective zones not accounted for in the traditional models (correlated convection cells, supergranulation?), or (iii) variability at higher frequencies aliased by our low sampling frequency.

For g Her, our observations might detect variability due to the propagation of waves excited by "classical" convective zone models, as well as high-order pulsation modes, since the Nyquist frequency of the observations is higher than all the listed theoretical frequencies. If the event observed on JD′ = 7772, happening within 14 days of a "quiet" period, is associated with the convection zone motions, these must be definitely "nonclassical" motions, since we have argued that this extra heating must have been localized. We suspect that this event is a result of convective overshooting from a very large supergranule cell which subtends somewhat less than 4π radians on the stellar surface. This picture is consistent with polarization measurements of late-type giant stars (e.g., Schwarz 1985). The absence of known magnetic activity on such evolved stars (Schrijver 1987) suggests that a solarlike prominence model is less appropriate.

5.3 Implications for Chromospheric Heating and Mass-Loss Processes

In our data there is no clear evidence for the existence of a strong, outwardly propagating shock wave, characterized by an enhanced emission in the line wings which in time propagates inwards towards the line core, or by the types of profile changes exhibited by Miras (Bookbinder *et al.* 1989; Brugel *et al.* 1992). Instead, our observations suggest that any shock waves generated by the photospheric variability or by very large scale convection motions modify the time-averaged structure of the outer atmosphere only marginally (cf., Eaton *et al.* 1990). The Ca II and Mg II line-forming regions of these semiregular stars appear to consist of a "steady-state" chromosphere through which large scale disturbances propagate.

The existence of a "steady-state" chromosphere varying only slightly ($< \pm 10\%$) with time, and which does not depend strongly on the observed photometric behavior, suggests the following. (i) The dominant modes of energy propagation leading to chromospheric heating are not in long-period waves ($P >$ weeks) associated with the observed photometric variability. This is in sharp contrast to the case of larger amplitude variables (e.g., Bookbinder *et al.* 1989; Brugel *et al.* 1992). (ii) Similarly, heating events occurring on scales associated with very large supergranule cells are probably not the source of the bulk of the chromospheric heating in these stars. However, in g Her (the most luminous star in our sample), we find evidence for a localized heating event amounting to 25% of the total chromospheric heating which may result from the overshooting of a large supergranule cell. (iii) The length scales of the processes leading to chromospheric heating (wavelengths of wave modes and/or source distributions) must be *substantially less than a stellar radius*, since otherwise we might expect to see some coherent structures evolve with time in our observations. (iv) If the dominant modes of propagation of energy are in acoustic waves, then this picture is consistent with the calculations of Cuntz

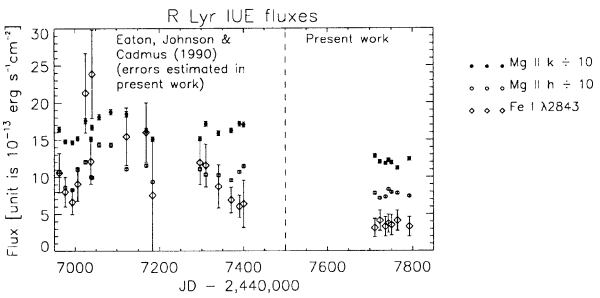

FIG. 13. Variations in the integrated fluxes of the Mg II and Fe I λ2843 lines in the time series spectra of R Lyr, using our data and those from Table 6 of Eaton *et al.* (1990). We remeasured some of the data of these authors using archival spectra, and estimated uncertainties from the signal-to-noise ratios of these data in the same way.

(1990). Cuntz (1992) has recently computed an *ab initio* model for the supergiant α Ori (M2 Iab) based upon stochastic shock waves. The characteristics of this model may in principle reproduce the type of observations of the giant stars obtained here. An initial comparison of the predictions of such models with *Hubble Space Telescope* observations of α Tau (K5 III) (Judge & Cuntz 1993) has, however, revealed potential problems. Further theoretical work is needed and is in progress.

Point (i) stands in contrast to models based purely upon energy generation through photospheric pulsation (Bowen 1988). It should be noted, however, that Bowen's (1988) calculations (which include only a crude treatment of the energy balance), in the absence of dust opacity, can produce a steady-state "calorisphere" (Willson 1988) which will lead to emission in chromospheric lines. However, this "calorisphere" resides several stellar radii above the photosphere. It is very unlikely that densities in such regions (if they exist in reality) are high enough to account for the observed chromospheric energy fluxes in our targets. Such a model cannot easily explain why these stars have similar "basal" chromospheric energy fluxes to less evolved stars on the giant branch which show much weaker photospheric variability.

Initially we had hoped to observe the effects of propagation of disturbances into the stellar wind. However, strong circumstellar absorption by lines of Fe I and Mn I and in the interstellar medium obscures changes in the Mg II line cores formed in the stellar winds. The Ca II lines hold greater promise since we were able to detect changes in the line profiles formed in the line cores in two of our target stars.

5.4 Relationship to Previous and Future Studies

Our results complement those of Eaton *et al.* (1990). Our data confirm some of their conclusions. However, we have re-examined their data for R Lyr to investigate how our work relates to theirs, and to attempt to determine whether claims that lines of Mg II, Al II], and Fe I vary differently as a function of time. Figure 13 shows data taken directly from Table 6 obtained by Eaton *et al.* (1990) together with our data. We remeasured several archived spectra of Eaton *et al.* (1990) using the procedures outlined above, and found agreement with their tabulated fluxes of h and k lines to within $\pm 2\%$. Furthermore, we estimated uncertainties of the weak Fe I lines by determining peak signal-to-noise ratios as done for our data. Our data were obtained at epochs when all chromospheric line fluxes were substantially lower (by $\sim 25\%$) than those observed by Eaton *et al.* (1990). It therefore appears that longer-term chromospheric variability (time scales $\geqslant$ years) is also present in R Lyr. Our data have generally lower signal-to-noise ratios than those of Eaton *et al.* (1990). However, we find that the uncertainties in the Fe I (and Al II]) line fluxes are too large to infer anything about relationships between the Mg II and other line fluxes from these datasets.

There are also theoretical reasons for doubting the existence of time delays between chromospheric lines when the variability is determined by chromospheric (and not circumstellar) phenomena. Eaton *et al.* (1990) argue that, owing to the great differences between the optical depths of, e.g., the Al II] and Mg II lines, the integrated fluxes are determined by different regions of the outer atmosphere. While this is certainly true for *monochromatic* fluxes, such a statement is incorrect for quantities integrated over the entire emission line profile, because these are controlled by the *thermalization depth* of the line (e.g., Mihalas 1978) and not the monochromatic optical depth. The thermalization lengths of all the lines discussed here are greater than the thickness of the chromosphere (Judge 1990). Thus, changes in the integrated flux of the chromospheric Al II] and Fe I lines would be expected to follow changes in the much more opaque Mg II lines.

We find little evidence for "lags" between chromospheric and photospheric fluxes in our dataset, which has a higher sampling rate but fewer points than discussed by Eaton *et al.* (1990). Therefore, we may well have missed phase shifts between photospheric and chromospheric variability larger than, say 0.3. However, we point out that the claimed lag of the Mg II emission fluxes behind the photospheric fluxes of ~ 35 days in the SRb star W Cyg (period ~ 131d) shown in Fig. 5 of Eaton *et al.* (1990), looks much less convincing when their entire dataset is considered (their Fig. 2). The same is true for the other stars in their dataset. We suggest that conclusions of Eaton *et al.* (1990) concerning phase shifts, wave propagation speeds, and length scales, be reconsidered in the light of the need for more complete observational studies.

Directions for future work should include (i) analyzing *IUE* data of α Ori (M2 Iab) using the techniques presented here, (ii) obtaining data over longer time scales, (iii) obtaining simultaneous spectropolarimetry and high dispersion spectra of these stars, (iv) obtaining better models of the convection zones for low-gravity stars and applying these to the study of wave propagation in the outer atmospheres, (v) obtaining very high dispersion Mg II profiles with the *Goddard High Resolution Spectrograph* on the *Hubble Space Telescope*.

P.G.J. and M.C. are grateful to NASA for funding the study of *IUE* spectra of cool giants through Grant Nos. NAG5-1145 and NAG5-1374 to the University of Colorado, and to the National Science Foundation and High Altitude Visitor's Program for funding and facilities. We are indebted to Mike Seeds and the program at Mt. Hopkins observatory for obtaining the photometric data needed for this study, to Mario Perez for an illuminating discussion of the photometric properties of the FES on *IUE*, and to Verne Smith for kindly obtaining spectra at the McDonald Observatory for us. We thank Paul Avellar for obtaining the McMath data during the course of the synoptic program. D.G.L. thanks David Jaksha for instructions on the operation of the McMath telescope.

REFERENCES

Allen, C. W. 1973, Astrophysical Quantities, 3rd Ed. (Athlone, London)
Antia, H. M., Chitre, S. M., & Narasimha, D. 1984, ApJ, 282, 574
Athay, R. G. 1976, The Solar Chromosphere and Corona: Quiet Sun (Reidel, Dordrecht)
Ayres, T. R. 1984, ApJ, 284, 784
Ayres, T. R. 1991, private communication
Bernat, A. P. 1981, ApJ, 246, 184
Bernat, A. P., & Lambert, D. L. 1976, ApJ, 204, 830
Bohn H. U. 1981, Ph. D. thesis, University of Würzburg
Bohn H. U. 1984, A&A, 136, 338
Bookbinder, J., Brugel, E. W., & Brown, A. 1989, ApJ, 342, 516
Bowen, G. H. 1988, ApJ, 329, 299
Brugel, E. W., Willson, L. A., Bowen, G. H., & Magalhães, M. 1992, preprint
Carpenter, K. G. 1992, The Seventh Cambridge Workshop on Cool Stars, Stellar Systems and the Sun, edited by J. Bookbinder and M. Giampapa, PASP Conf. Series 26, p. 17
Corliss, C. H., & Tech, J. L. 1968, Oscillator Strengths and Transition Probabilities for 3288 Lines of Fe I, NBS Monograph 108
Cuntz, M. 1987, A&A, 188, L5
Cuntz, M. 1990, ApJ, 349, 141
Cuntz, M. 1992, in Proceedings of the Seventh Cambridge Workshop on Cool Stars, Stellar Systems and the Sun, edited by M. Giampapa and J. Bookbinder, A.S.P. Conf. Series, p. 383
Drake, S. A. 1985, in Progress in Stellar Spectral Line Formation Theory, edited by J. E. Beckman and L. Crivellari (Reidel, Dordrecht), p. 351
Drake, S. A., & Linsky, J. L. 1983, ApJ, 273, 299
Drake, S. A., Brown, A., & Linsky, J. L. 1984, ApJ, 284, 774
Dupree, A. K., Baliunas, S. L., Guinan, E. F., Hartmann, L., Nassiopoulos, G. E., & Sonneborn, G. 1988, in A Decade of UV Astronomy with the IUE Satellite, ESA SP-281, Vol. 1., p. 365
Eaton, J. A., & Johnson, H. R. 1988, ApJ, 325, 355
Eaton, J. A., Johnson, H. R., & Cadmus, R. 1990, ApJ, 364, 259
Eriksson, K., Gustafsson, B., Johnson, H. R., Querci, F., Querci, M., Baumert, J. H., Carlsson, M., & Olofsson, H. 1986, A&A, 161, 305
Fireman, G. F., & Imhoff, C. L. 1989, IUE Newsletter No. 40, 10
Goldberg, L. 1979, QJRAS, 20, 361
Guinan, E. F. 1990, in Evolution in Astrophysics, edited by E. Rolfe, ESA SP-310, p. 73
Harper, G. M. 1990, MNRAS, 243, 381
Hobbs, L. M. 1974, ApJ, 191, 381
Hoffleit, D., & Jaschek, C., 1984, The Bright Star Catalog, 4th Rev. Ed. (Yale University, New Haven)
Holzer, T. E., & MacGregor, K. B. 1985, in Mass-Loss from Red Giants, edited by M. Morris and B. Zuckerman (Reidel, Dordrecht), p. 229
Imhoff, C. L. 1989, IUE Newsletter No. 40, 5
Jaksha, D. 1989, private communication
Johnson, H. R. 1987, in Proceedings of the Fifth Cambridge Workshop on Cool Stars, Stellar Systems and the Sun, edited by J. L. Linsky and R. E. Stencel (Springer, Berlin), p. 399
Jorås, P. 1989, D. Scient. thesis, University of Oslo
Jordan, C., & Linsky, J. L. 1987, in Exploring the Universe with the IUE Satellite, edited by Y. Kondo (Reidel, Dordrecht), p. 259
Judge, P. G. 1986, MNRAS, 221, 119
Judge, P. G. 1989, in The Evolution of Peculiar Red Giant Stars, IAU Colloquium No. 106, edited by H. R. Johnson and B. Zuckerman (Cambridge University Press, Cambridge), p. 303
Judge, P. G. 1990, ApJ, 348, 279
Judge, P. G., & Cuntz, M. 1993, ApJ (in press)
Judge, P. G., & Stencel, R. E. 1991, ApJ, 371, 357
Jura, M. 1986, Ir. Astron. J. 17, 322
Kholopov, P. N., *et al.* 1985, General Catalogue of Variable Stars, Fourth Ed., Vol. I-III (Nauka, Moscow)
Lovy, D., Maeder, A., Noëls, A., & Gabriel, M. 1984, A&A, 133, 307
Malagoli, A., Cattaneo, F., & Brummel, N. H. 1990, ApJ, 361, L33
Mihalas, D. 1978, Stellar Atmospheres (Freeman, San Francisco)
Schrijver, C. J. 1987, A&A, 172, 111
Schwarz, H. E. 1985, A&A, 147, 111
Schwarzschild, M. 1975, ApJ, 195, 137
Stencel, R. E. 1977, ApJ, 215, 176
Taylor, D. 1990, IUE Newsletter No. 41, 10
Ulmschneider, P., Priest, E. R., & Rosner, R. 1991, Mechanisms of Chromospheric & Coronal Heating (Springer, Berlin)
van der Veen, W. E. C. J., & Habing, H. J. 1988, A&A, 194, 125
Willson, L. A. 1988, in Pulsation and Mass Loss in Stars, edited by R. Stalio and L. A. Willson (Kluwer, Dordrecht), p. 285
Younger, S. M., Fuhr, J. R., Martin, G. A., & Wiese, W. L. 1978, J. Phys. Chem. Ref. Data 7, 495